Electronic Supplementary Material (ESI) for Journal of Materials Chemistry B.
This journal is © The Royal Society of Chemistry 2014

Supporting Information

Supramolecular nanoparticle carriers self-assembled from cyclodextrin- and adamantane-functionalized polyacrylates for tumor-targeted drug delivery

Chung Yen Ang,[a] Si Yu Tan,[a] Xiaoling Wang,[b] Quan Zhang,[a] Majad Khan,[c] Bai Linyi,[a] Subramanian Tamil Selvan,[d] Xing Ma,[e] Liangliang Zhu,[a] Kim Truc Nguyen,[a] Nguan Soon Tan,*[,b,f] Yanli Zhao*[,a,e]

[a]Division of Chemistry and Biological Chemistry, School of Physical and Mathematical Sciences, Nanyang Technological University, 21 Nanyang Link, Singapore 637371, Singapore

[b]School of Biological Sciences, Nanyang Technological University, 60 Nanyang Drive, Singapore 637551, Singapore

[c]Institute of Bioengineering and Nanotechnology, 31 Biopolis Way, Singapore 138669, Singapore

[d]Institute of Material Research and Engineering, 3 Research Link, Singapore 117602, Singapore

[e]School of Materials Science and Engineering, Nanyang Technological University, 50 Nanyang Avenue, Singapore 639798, Singapore

[f]Institute of Molecular and Cell Biology, 61 Biopolis Drive, Proteos, A*STAR, Singapore 138673.

[†]These authors equally contributed to this work.

Table of Contents

1. Synthetic scheme of various components

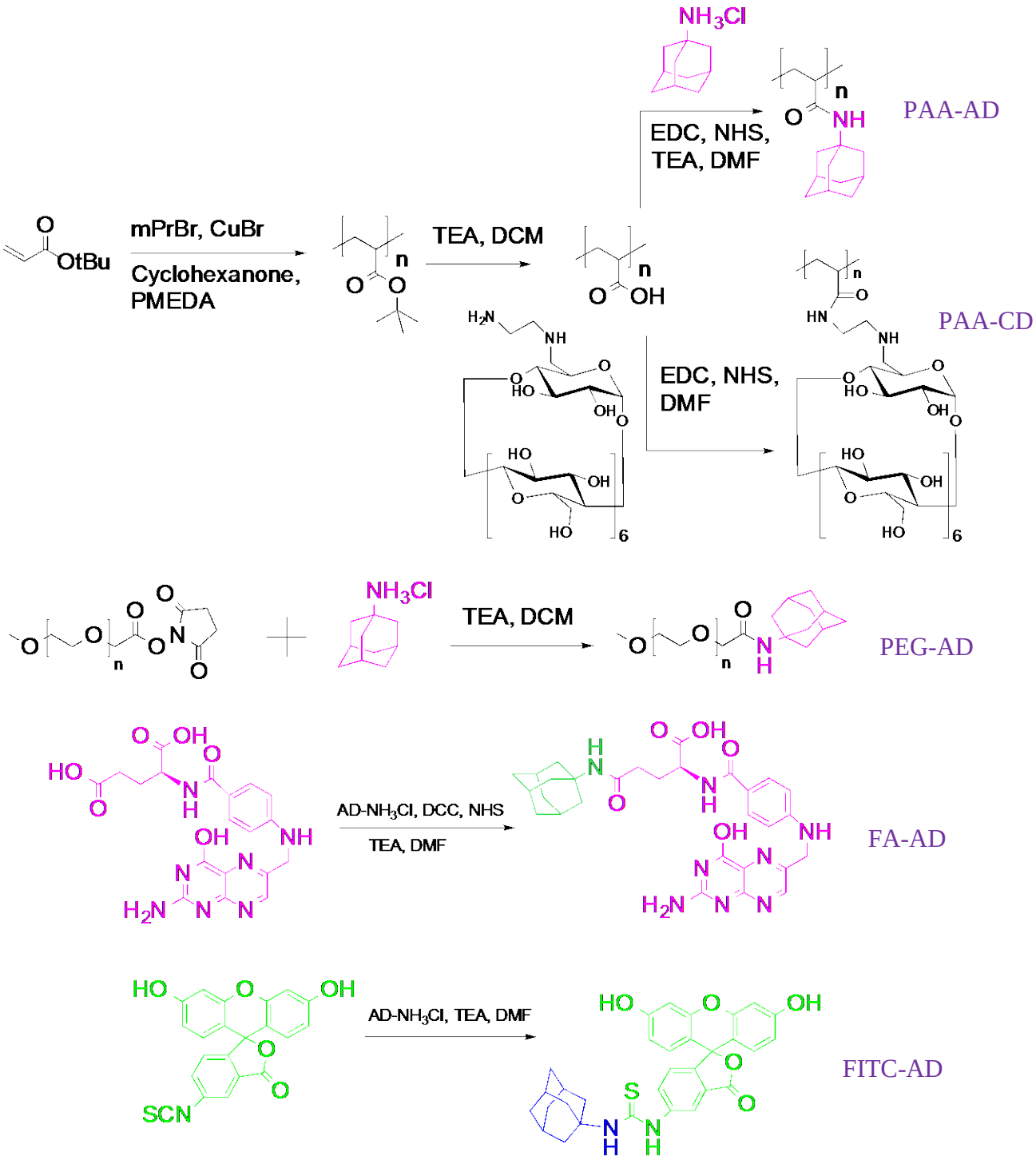

Scheme S1. Schematic representation for the synthesis of PAA-AD, PAA-CD, PEG-AD, FA-AD and FITC-AD.

2. Analysis of PAA-AD and PAA-CD

2.1 UV-Vis studies for determination of the conjugation degree of *β*-CD on PAA-CD

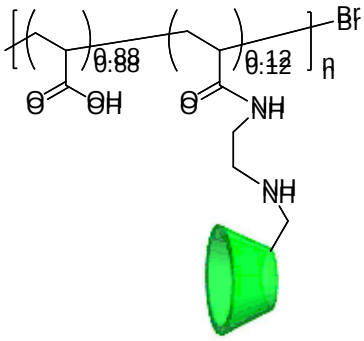

The conjugation degree of *β*-CD onto PAA was determined by the UV-Vis spectroscopy technique. As the *β*-CD molecule does not possess any UV-Vis absorption, conventional UV-Vis standard calibration plot for *β*-CD could not be prepared. Thus, we relied on an indirect UV-Vis spectroscopy method for the determination of the conjugation degree of *β*-CD on PAA-CD. The hydrophobic cavity of *β*-CD enables it to host a variety of guest molecules including azobenzene compound (Figure S2.1) with a certain binding constant. In a recent work,[1] the binding constants (*k*) of *β*-CD with azobenzene compounds were determined via the reciprocal plot of Hidebrand-Benesi equation (Figure S2.2). Upon complexation with *β*-CD, there is a significant change in the UV-Vis spectrum of azobenzene. The change of the absorbance can be used for the preparation of the reciprocal plot from the Hindebrand-Benesi equation as shown below.

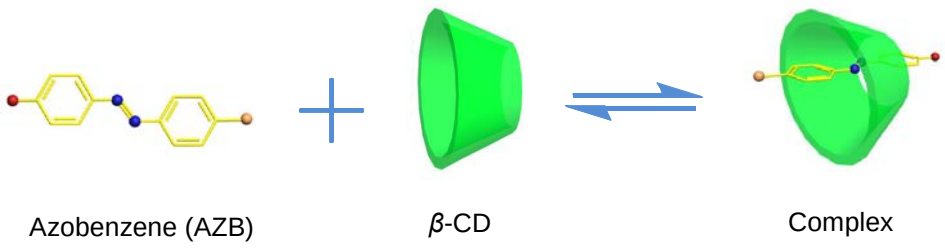

Figure S2.1. Schematic illustration for the complexation of *β*-CD with azobenzene.

a) $$k = \frac{[\text{Complex}]}{[\beta\text{−CD}][\text{AZB}]}$$

b) $$\frac{1}{|\Delta A|} = \frac{1}{\Delta\varepsilon k[AZB][\beta]} - \frac{1}{\Delta\varepsilon[AZB]}$$

|ΔA| is the modulus change in the abs of AZB upon the complexation with *β*-CD, Δε is the change in the molar extinction coefficient of AZB at the π-π* wavelength, *k* is the binding constant between AZB and *β*-CD, [AZB] is the concentration of AZB, and [*β*] is the concentration of *β*-CD.

Figure S2.2. Formation equilibrium of the *β*-CD/azobenzene complex. a) The expression of the reaction equilibrium. b) The reciprocal plot of the Hindebrand-Benesi equation.

The binding constant reveals the crucial information regarding the stability of the resultant complex, which is one of the determining factors for its self-assembly application. In this work, we relied on the reciprocal plot of the Hindebrand-Benesi equation as the standard calibration plot for the determination of the *β*-CD concentration in the given solution. Thereafter, the degree of conjugation on PAA can be calculated by taking the ratio of the absolute mole of *β*-CD to the absolute mole of PAA polymer. Owing to its excellent aqueous solubility, sodium 4-((4-hydroxyphenyl)diazenyl)benzenesulfonate (HBS) (Figure S2.3) was chosen as the azobenzene model molecule for the preparation of the reciprocal plot.

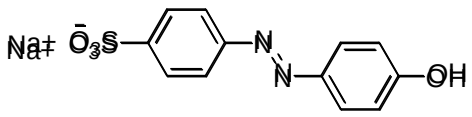

Figure S2.3. Molecular structure of sodium (*E*)-4-((4-hydroxyphenyl)diazenyl)benzenesulfonate (HBS).

<u>Preparation of Hindebrand-Benesi plot</u>

In the preparation of the reciprocal plot from the Hidebrand-Benesi equation, the UV-Vis spectrum of aqueous HBS (8.00 x 10^{-5} M, 3.0 mL) was measured in the absence of light. Thereafter, aqueous *β*-CD (20.0 mg mL^{-1}, 15 µL) was added to the same HBS solution and the UV-Vis spectrum of the resulting solution was measured again. This process was repeated by systematically adding aqueous *β*-CD (20.0 mg/mL) into the same solution, and the absorbance at 353 nm (π-π*) was recorded accordingly (Figure S2.4 and Table S2.1). Lastly, the reciprocal plot

of the Hindebrand-Benesi equation was prepared by plotting the values from the $\frac{1}{[\beta]}$ column versus the values from the $\frac{1}{|\Delta A|}$ column (Figure S2.5).

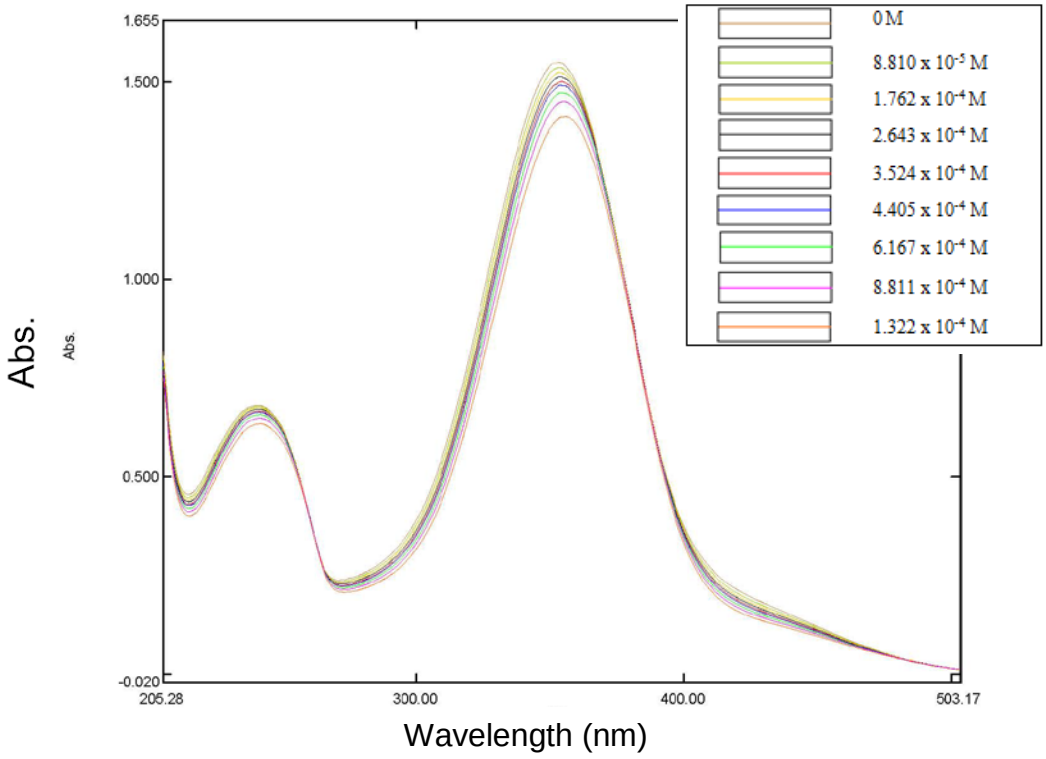

Figure S2.4. UV-Vis absorption spectra of HBS solution (8.00 x 10^{-5}M) containing various amount of β-CD.

Entry (n)	Volume of addition[a] (µL)	$[\beta]$[b] (mg mL^{-1})	$[\beta]$ (M)	$\frac{1}{[\beta]}$ (M^{-1})	Abs_{353} (A_n)	$\lvert\Delta A\rvert = \lvert A_n - A_0\rvert$	$\frac{1}{\lvert\Delta A\rvert}$
0	0	0	0	-	1.549	0	-
1	15	0.1	8.810 x 10^{-5}	11350	1.534	0.015	66.7
2	30	0.2	1.762 x 10^{-4}	5675	1.523	0.026	38.5
3	45	0.3	2.643 x 10^{-4}	3783	1.512	0.037	27.0
4	60	0.4	3.524 x 10^{-4}	2837	1.499	0.05	20.0
5	75	0.5	4.405 x 10^{-4}	2270	1.491	0.058	17.2
6	105	0.7	6.167 x 10^{-4}	1621	1.472	0.077	13.0
7	150	1	8.811 x 10^{-4}	1135	1.445	0.104	9.62
8	225	1.5	1.322 x 10^{-4}	756.7	1.408	0.141	7.09

[a] Aqueous β-CD with a concentration of 20.0 mg mL^{-1}, [b] final concentration of β-CD in the solution prior to UV-Vis spectroscopy measurement

Table S2.1. Conditions and results of the UV-Vis spectroscopy measurements for the preparation of the reciprocal plot from the Hindebrand-Benesi equation.

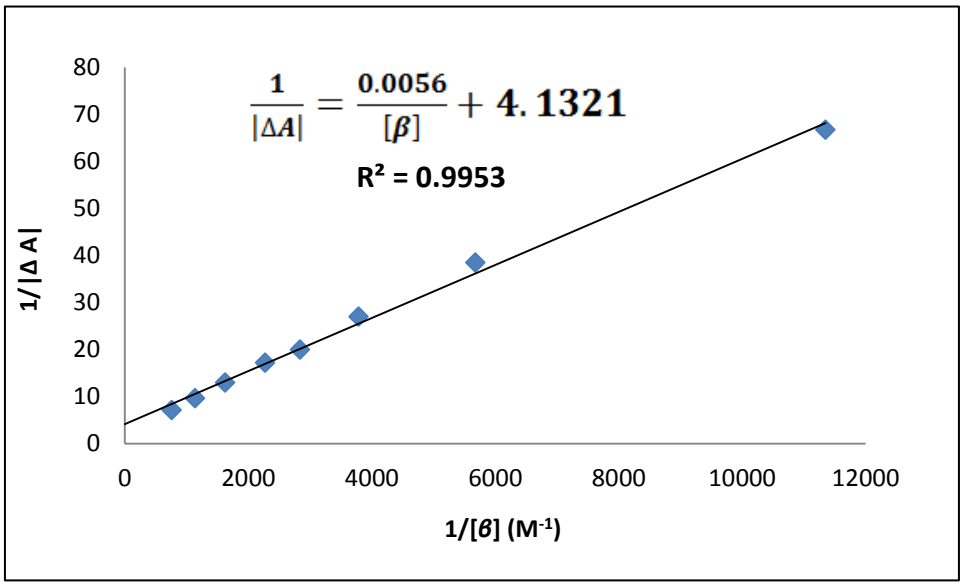

Figure S2.5. The reciprocal plot of the Hindebrand-Benesi equation for the complexation between HBS and *β*-CD.

Determination of the conjugation degree of *β*-CD on PAA-CD

The conjugation degree of *β*-CD onto PAA was determined indirectly through the use of UV-Vis spectroscopy technique. The determination was done by first measuring the absorbance of the HBS solution (8.00 x 10^{-5} M, 3.00 mL) in the absence of light. After which, aqueous PAA-CD (44 mg mL^{-1}, 50 µL) was added into the same HBS solution and the absorbance was measured once again under the same conditions (Figure S2.6). Thereafter, the difference in the absorbance at the wavelength of 353 nm was determined and applied onto the reciprocal plot of the Hindebrand-Benesi equation to obtain the concentration of *β*-CD in the polymer solution. Subsequently, the mass of the PAA polymer was calculated and the molar ratio of *β*-CD to the PAA polymer was determined, and this can be re-expressed as the conjugation degree of *β*-CD on PAA. The results of various measurements and calculations are summarized in Table S2.2.

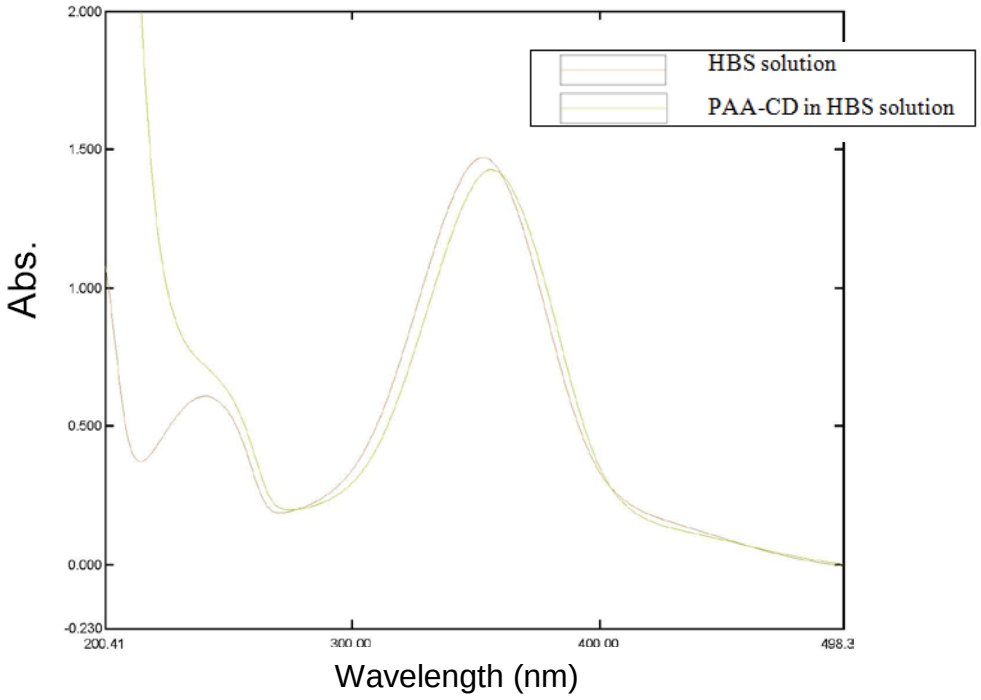

Figure S2.6. UV-Vis absorption spectra of HBS solution (8.00 x 10^{-5}M) with and without PAA-CD.

Abs_{353} of HBS solution in the absence of PAA-CD (A_0)	1.471
Abs_{353} of HBS solution in the presence of PAA-CD (A)	1.417
$\|\Delta \boldsymbol{A}\| = \|\boldsymbol{A} - \boldsymbol{A_0}\|$	0.054
$\boldsymbol{1}/_{\|\Delta \boldsymbol{A}\|}$	18.51
1/[β]	2567 M^{-1}
Concentration of β-CD in HBS solution (3 mL), [β]	3.895 x 10^{-4} M

Table S2.2. Results obtained from the UV-Vis spectroscopy measurement of the HBS solution containing the PAA-CD polymer.

After obtaining the concentration of β-CD from the HBS solution upon the titration of PAA-CD, the value was used to calculate the ratio between the moles of the β-CD molecule to the moles of PAA polymer. Based on the results obtained from this experiment, it was found that the ratio of β-CD to PAA polymer is approximately 3:1. The ratio obtained was then re-expressed as the conjugation degree of β-CD onto PAA and the value was calculated to be 12%.

Calculations

Concentration of β-CD in 3 mL of HBS solution, [β] = 3.895 x 10^{-4} M

Concentration of β-CD in 50 µL of PAA-CD solution = 3.895 x 10^{-4} M x $\frac{3000\mu L \text{ x}}{50\mu L}$

= 0.02337 M

Mass of β-CD in 50 µL of PAA-CD solution = 0.050 mL x 0.02337 M x 1177 $\frac{mg}{/mmol}$

= 1.375 mg

Mass of PAA-CD in 50 µL of PAA-CD solution = 44 $\frac{mg}{/mL}$ x 0.050 mL

= 2.2 mg

Of 2.2 mg of PAA-CD, mass contributed from PAA backbone = 2.2 mg – 1.375 mg

= 0.83 mg

Mole of PAA in 0.83 mg = $\frac{0.83\,mg/}{1983\,\frac{mg}{/mmol}}$ = 0.419 µmol

Mole of β-CD in the same 50 µL of PAA-CD solution = 0.050 mL x 0.02337 M = 1.168 µmol

Mole ratio of β-CD to PAA = $\frac{1.168\mu mol/}{0.419\mu mol}$ = 2.79 : 1 ≈ 3 : 1

Number of conjugation sites per PAA = 25

Conjugation density = $\frac{3}{25} \times 100\% = 12\%$

2.2 Conjugation degree of AD on PAA evaluated through MALDI-TOF MS

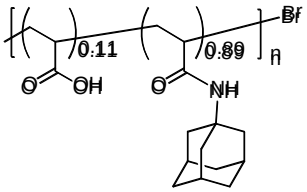

The conjugation degree of AD on PAA was calculated based on the result obtained from MALDI-TOF MS. The *m/*z value obtained from MALDI-TOF MS of PAA-AD was 4924. The *m/*z value of PAA was 1952 and thus there are 25 repeat units on the synthesized PAA.

Define the number of conjugation site of AD onto PAA to be *n*:

Molecular weight of AD-NH_2 = 151

Molecular weight of the MBrP initiator = 183

Molecular weight of every repeat unit of acrylic acid = 72

Molecular weight of PAA-AD will be:

$$183 + 72 \times 25 - n \times 18 + n \times 151 = 4924$$

Solving for *n* gives *n* = 22

Thus, percent conjugation = $\frac{22}{25} \times 100\% = 89\%$

3. Electron microscopy studies

3.1 Transmission electron microscope (TEM) studies

The morphology and size of the self-assembled nanoparticles were studied by TEM. The TEM samples were prepared by dropping the sample solution (10 µL) onto pieces of hydrophilic copper grids. Excess amount of liquid was absorbed and removed by a piece of filter paper. The sample grids were then allowed to dry overnight and directly taken for TEM studies. No staining was involved for all TEM studies.

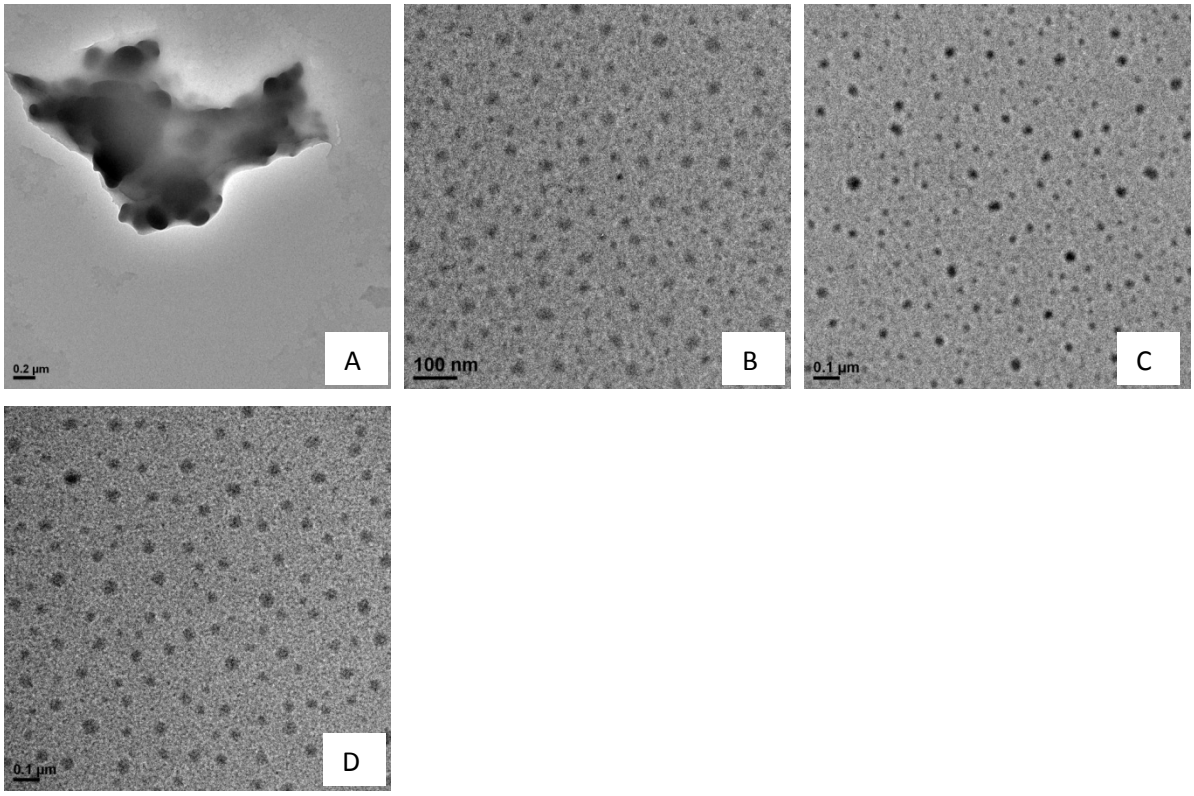

Figure S3.1. TEM images of A) polymeric aggregates prepared from the mixture of PAA-CD and PAA-AD without the addition of PEG-AD, B) ZG-01 (FA+VE) NPs, C) ZG-02 NPs, and D) ZG-01 (FA+VE) NPs after the treatment with 1M acetate buffer (pH 5.5).

3.1 Scanning electron microscope (SEM) studies

The morphology and size of the self-assembled nanoparticles were also studied by SEM. The SEM samples were prepared by dropping the sample solution (10 µL) onto pieces of double coated conductive carbon tapes. Excess amount of liquid was drained off and the tapes were dried with compressed air. The process was repeated for 3 times before a layer of gold was sputtered on top of the samples for SEM studies.

4. Confocal fluorescence microscopy images

A

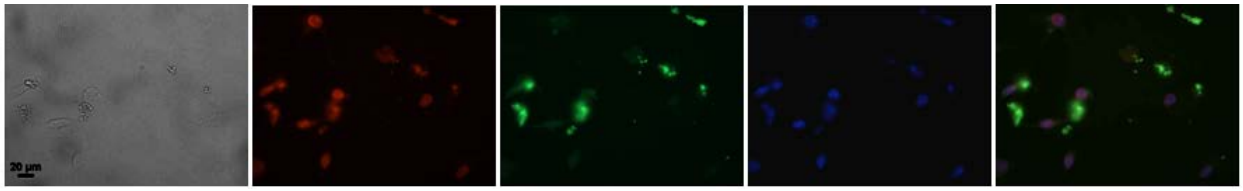

B

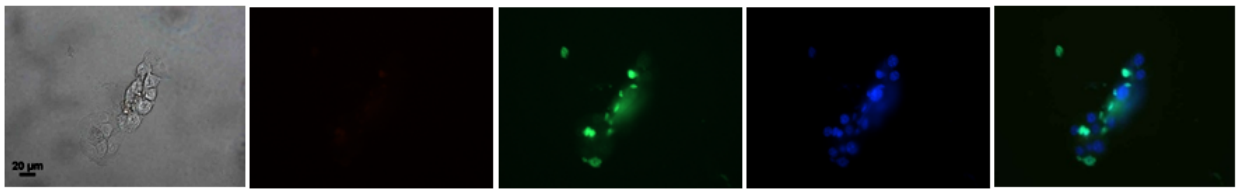

C

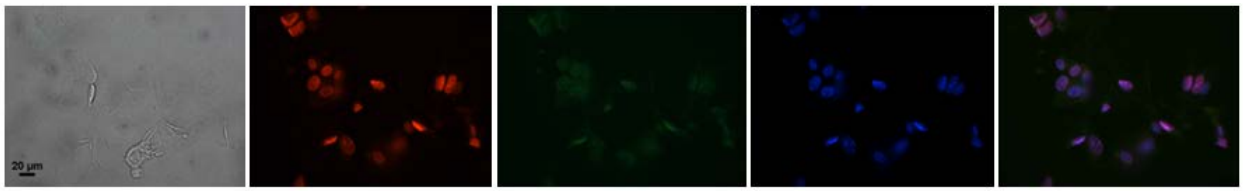

Figure S4.1. Confocal fluorescence microscope images of MDA-MB231 cells upon treatment with A) ZG-01 (FA+VE) NPs (0.6 mg mL^{-1}), B) ZG-02 NPs (0.6 mg mL^{-1}) and C) Free DOX (30 µg mL^{-1}) after 4 hours incubation, visualizing (from left to right) the bright field image of the cells followed by DOX channel (excitation filter: 540/25 nm; emission filter: 605/55 nm), FITC channel (excitation filter: 480/40 nm; emission filter: 535/50 nm), DAPI channel (excitation filter: 350/50 nm; emission filter: 460/50 nm), and merged images of all fluorescence images within the cellular compartments.

Confocal fluorescence images of MDA-MB231 cells under various conditions were presented in Figure S4.1. The multiple red and green spots on Figure S4.1A indicate that there was an efficient uptake of the ZG-01 (FA+VE) NPs by the cells. Figure S4.1B confirmed that folic acid can mediate the endocytosis of the ZG-02 NPs, in which DOX was absence in the NP system. Lastly, Figure S4.1C shows that there was a positive uptake of free DOX by MDA-MB231 cells.

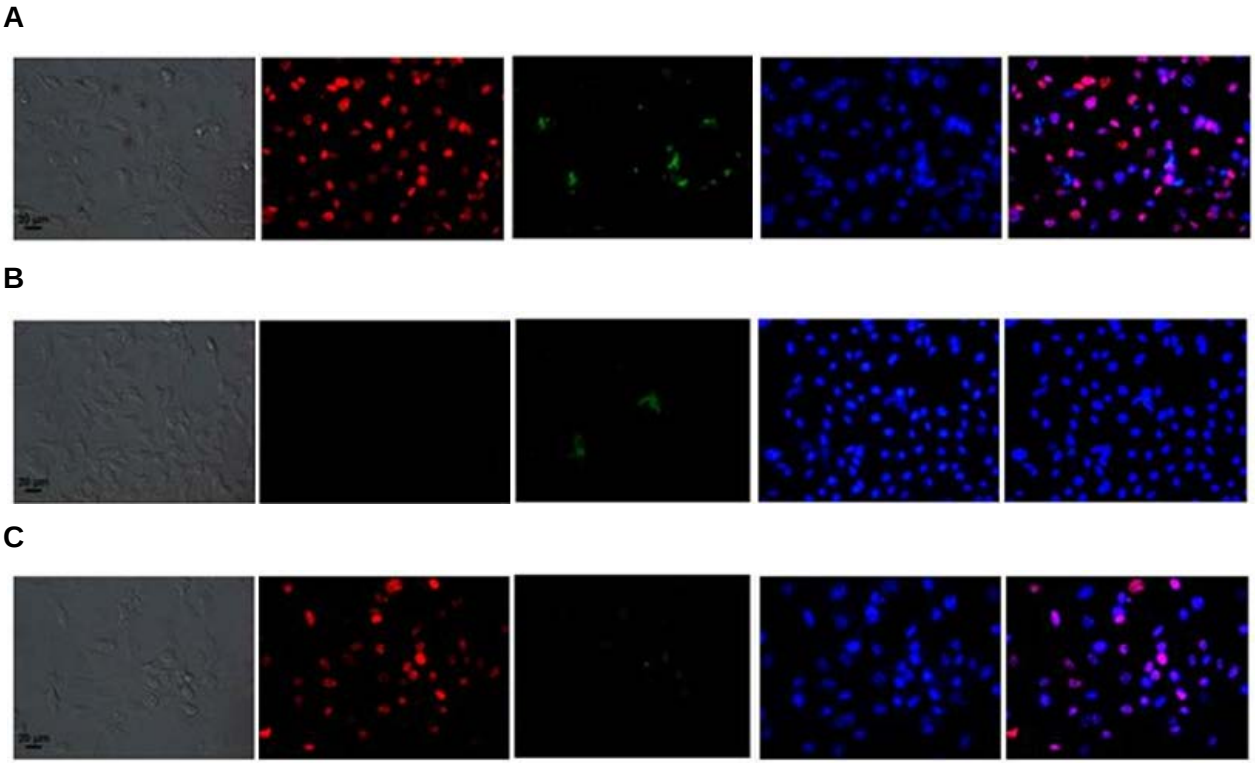

Figure S4.2. Confocal fluorescence microscope images of B16-F10 cells upon treatment with A) ZG-01 (FA+VE) NPs (0.6 mg mL^{-1}), B) ZG-02 NPs (0.6 mg mL^{-1}) and C) free DOX (30 µg mL^{-1}) after 4 hours incubation, visualizing (from left to right) the bright field image of the cells followed by DOX channel (excitation filter: 540/25 nm; emission filter: 605/55 nm), FITC channel (excitation filter: 480/40 nm; emission filter: 535/50 nm), DAPI channel (excitation filter: 350/50 nm; emission filter: 460/50 nm), and merged images of all fluorescence images within the cellular compartments.

Confocal fluorescence images of B16-F10 cells under various conditions were presented in Figure S4.2. Similar to the fluorescence images of MDA-MB231 cells, the multiple red and green spots on Figure S4.2A indicate that there was an efficient uptake of the ZG-01 (FA+VE)

NPs by the cells. Figure S4.2B confirmed that folic acid can mediate the endocytosis of the ZG-02 NPs, in which DOX was absence in the NP system. Lastly, Figure S4.2C shows that there was a positive uptake of free DOX by B16-F10 cells.

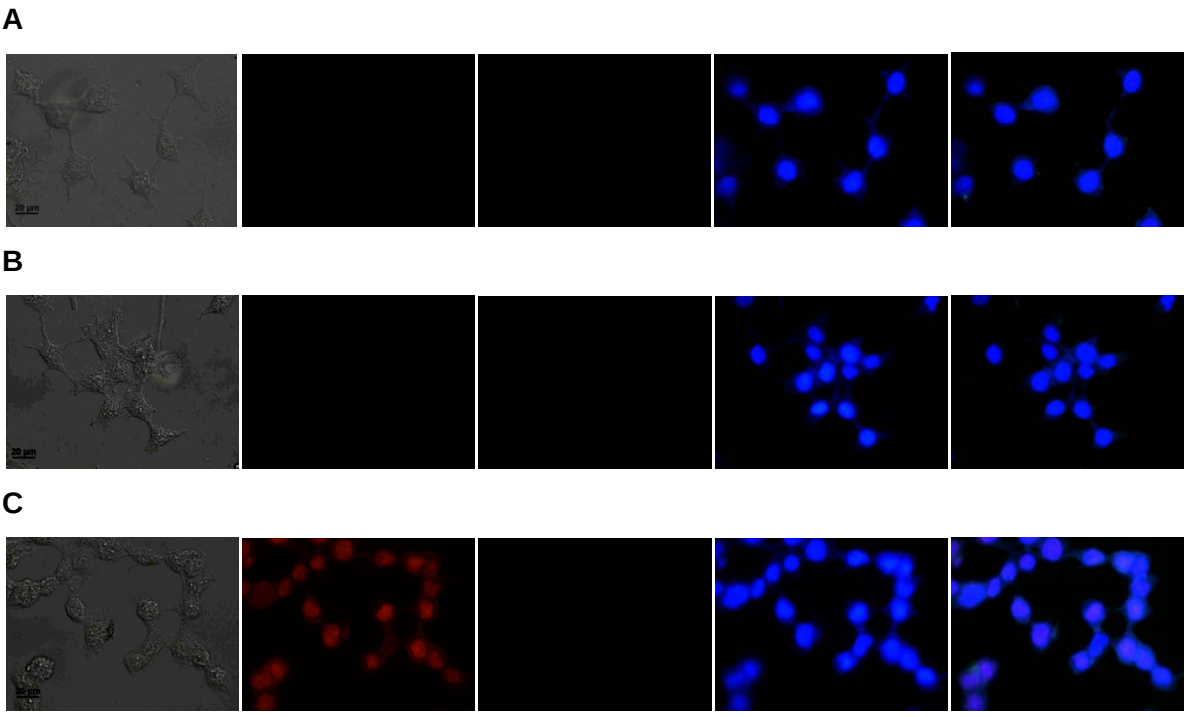

Figure S4.3. Confocal fluorescence microscope images of HEK293 cells upon treatment with A) ZG-01 (FA+VE) NPs (0.6 mg mL^{-1}), B) ZG-02 NPs (0.6 mg mL^{-1}) and C) free DOX (30 µg mL^{-1}) after 4 hours incubation, visualizing (from left to right) the bright field image of the cells followed by DOX channel (excitation filter: 540/25 nm; emission filter: 605/55 nm), FITC channel (excitation filter: 480/40 nm; emission filter: 535/50 nm), DAPI channel (excitation filter: 350/50 nm; emission filter: 460/50 nm), and merged images of all fluorescence images within the cellular compartments.

Confocal fluorescence images of HEK293 cells under various conditions were presented in Figure S4.3. In this set of imaging experiments, only the cell image from the treatment of free DOX shows positive signal of DOX within the cellular endoplasm, while the remaining two sets of images do not show signals of DOX or NPs within the cells. The experiments conclude that the absence of folate receptor on the HEK293 cell surface prevents the non-specific delivery of DOX into the healthy cell line. Together with imaging experiments from the two cancerous cell

lines, it was confirmed that the NP system has the ability to perform target-specific drug delivery towards cancerous MDA-MB231 and B16-F10 cells, while preventing the non-specific uptake of the anticancer drug by healthy cells.

5. Histology studies of various organs of mice

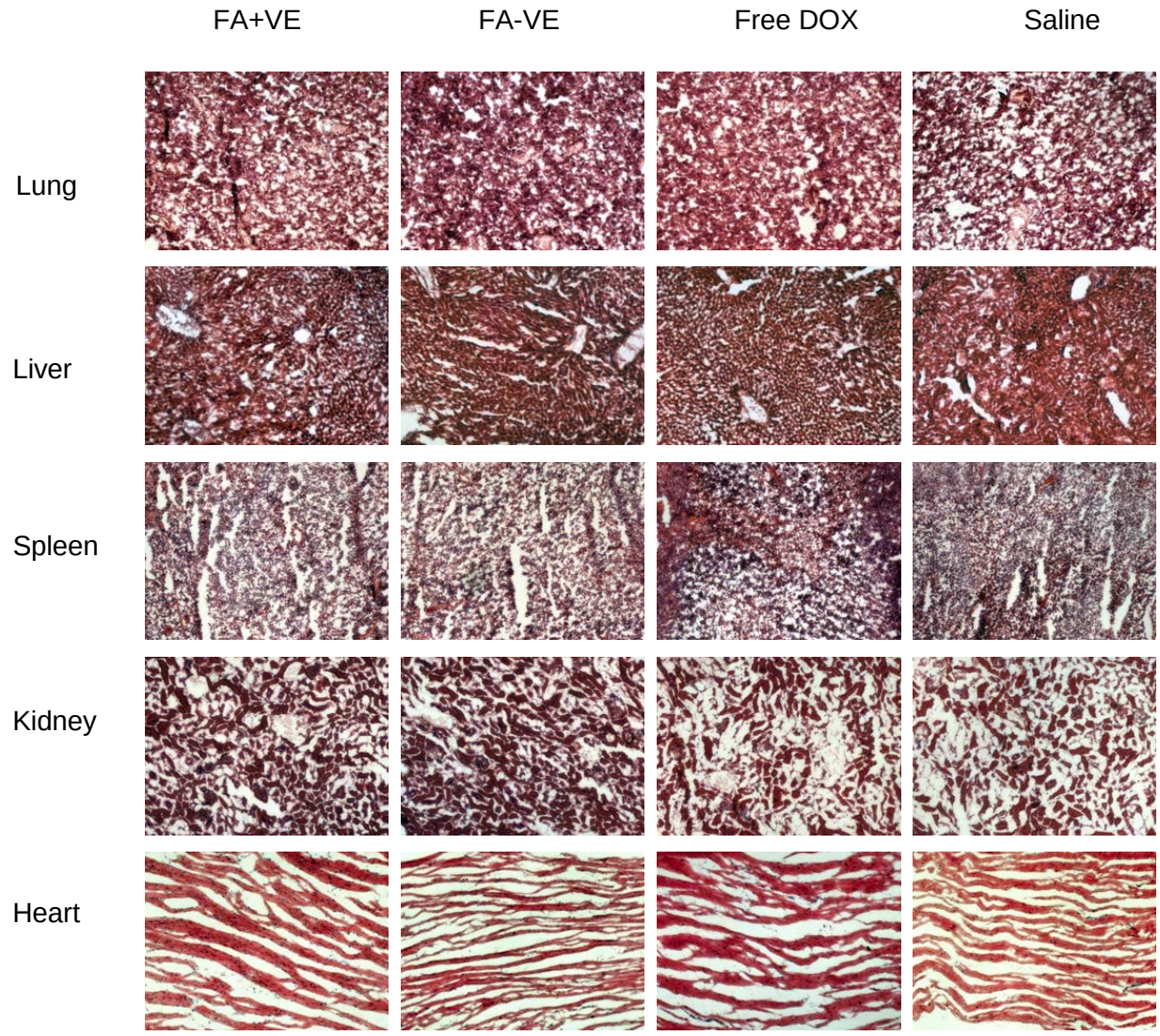

Figure S5. H&E staining images of major organs from mice treated with various samples. No obvious differences are observed from these images.

6. Spectroscopic and chromatographic data of various compounds

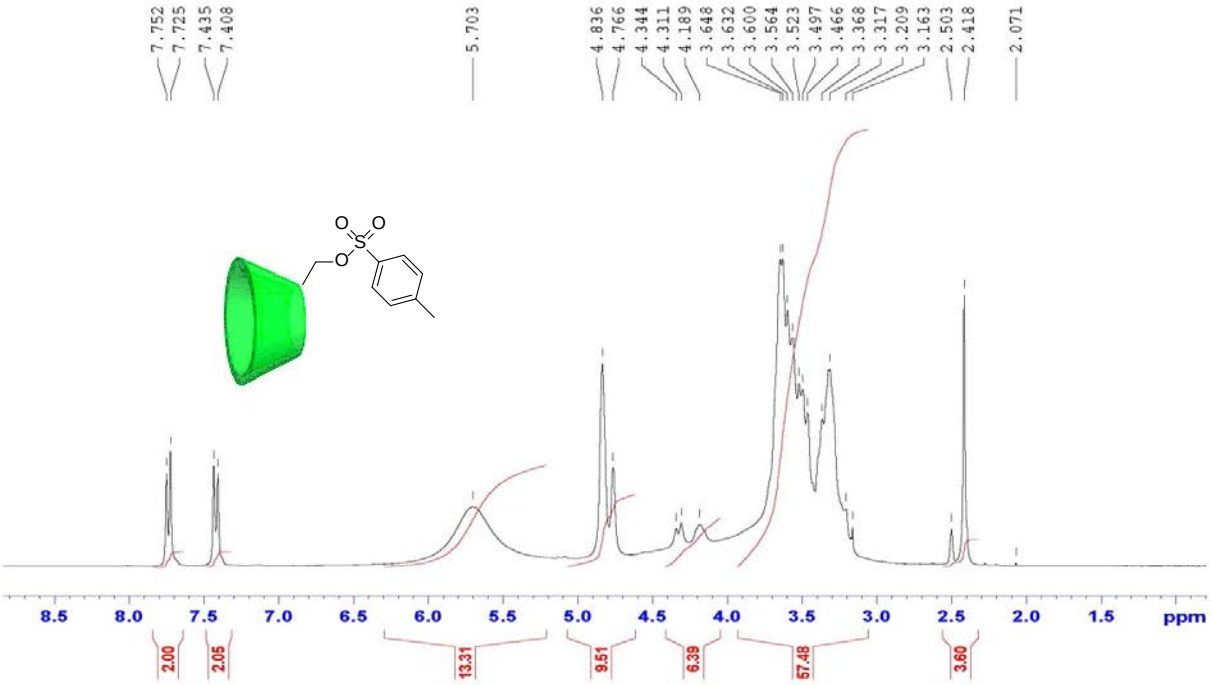

Figure S6.1. ^{1}H NMR spectrum of mono-6-deoxy-6-(*p*-toluenesulfonyl)-*β*-CD.

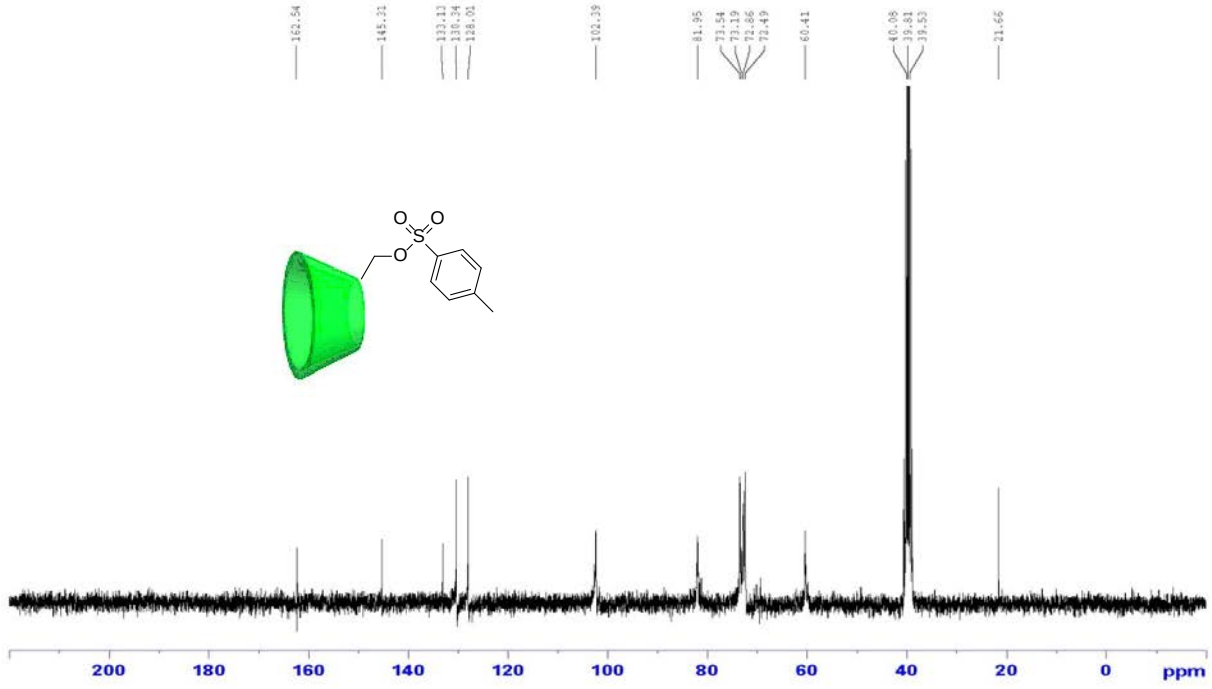

Figure S6.2. ^{13}C NMR spectrum of mono-6-deoxy-6-(*p*-toluenesulfonyl)-*β*-CD.

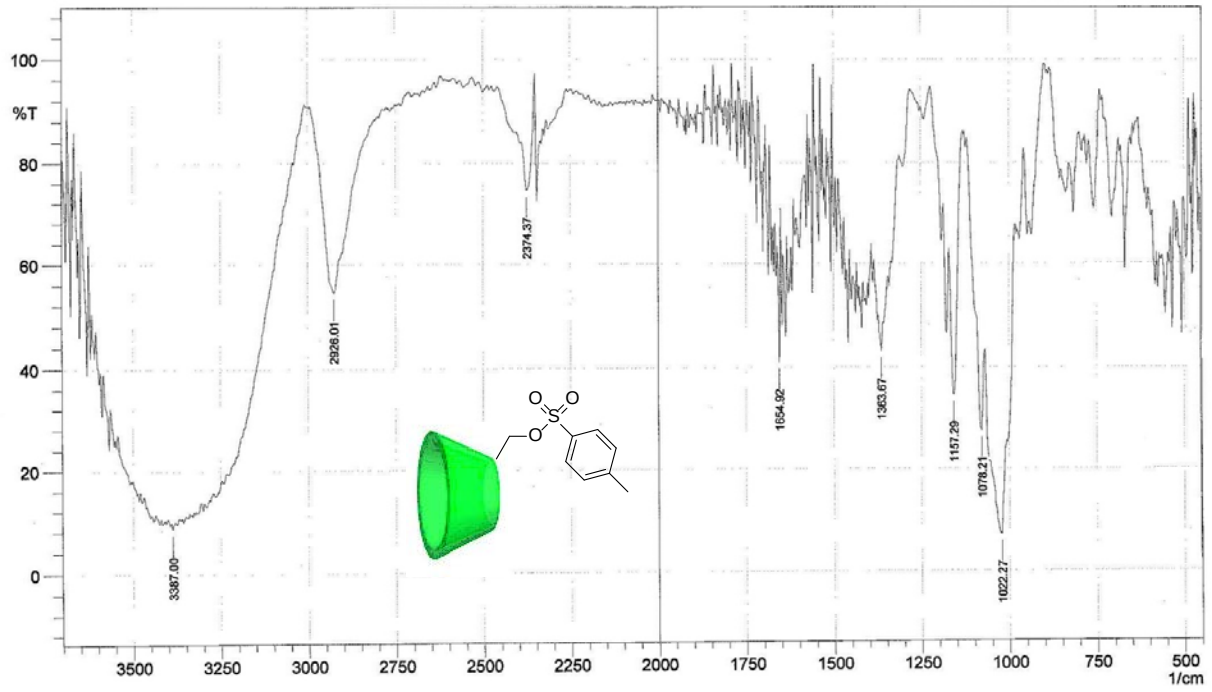

Figure S6.3. IR spectrum of mono-6-deoxy-6-(*p*-toluenesulfonyl)-*β*-CD.

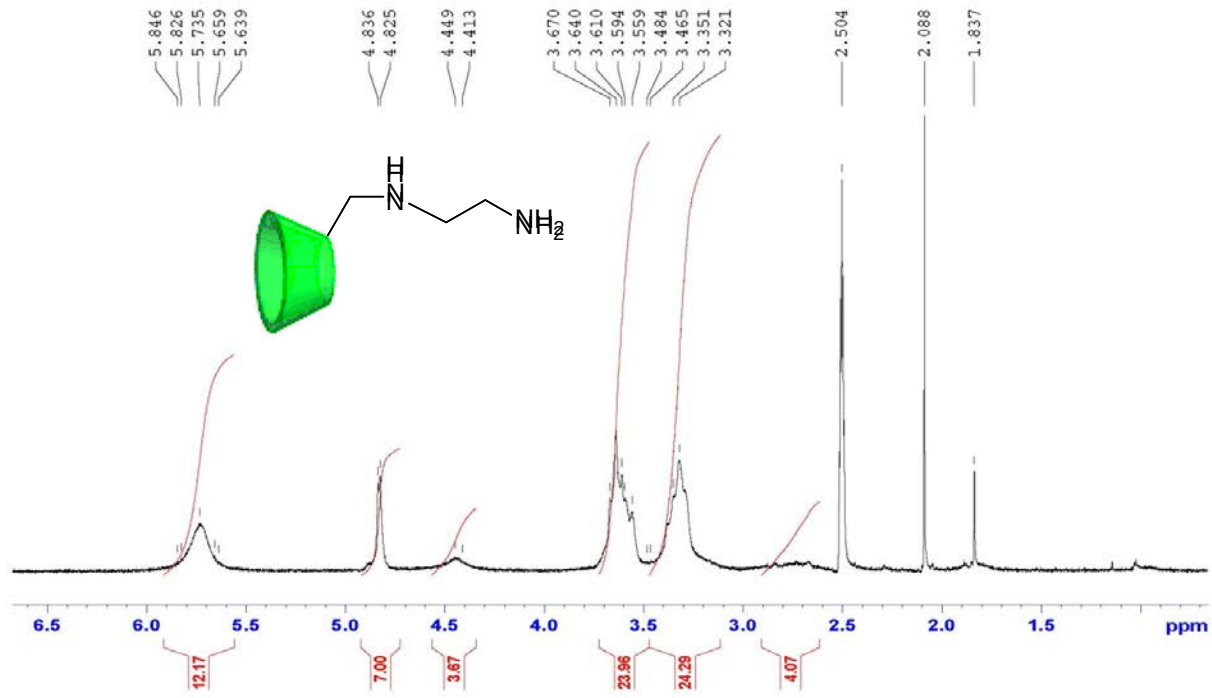

Figure S6.4. ^{1}H NMR spectrum of 6-mono-(*N*-aminoethyl) amino-*β*-CD.

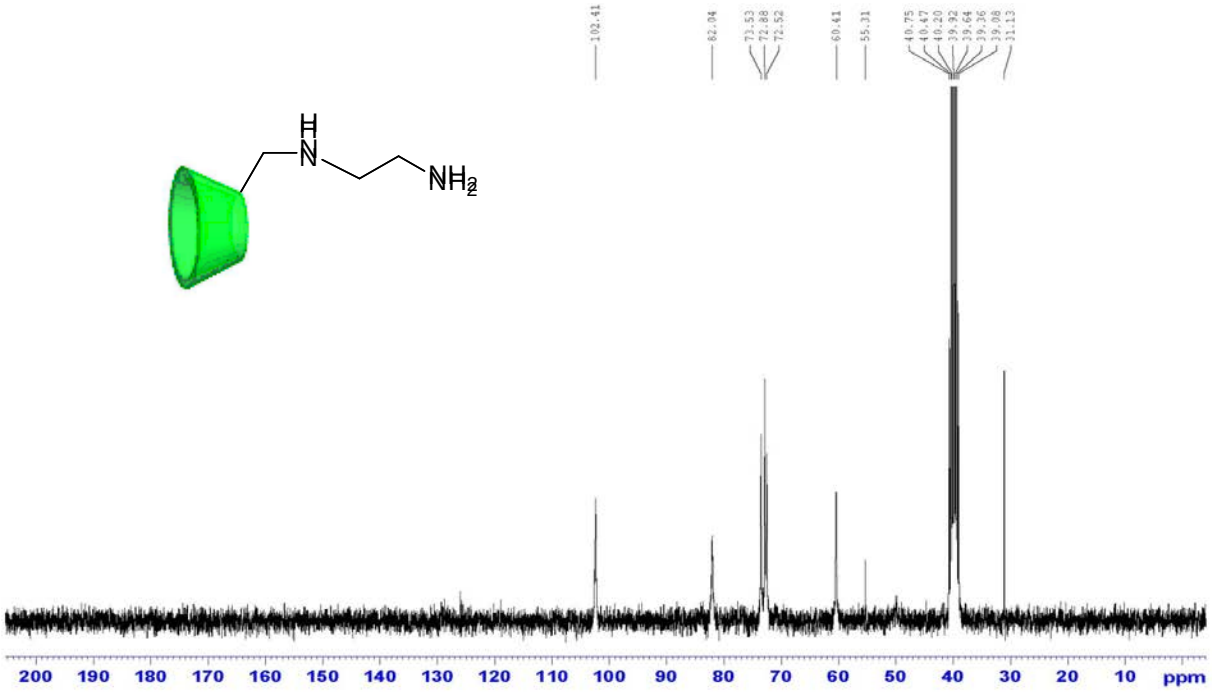

Figure S6.5. ^{13}C NMR spectrum of 6-mono-(*N*-aminoethyl) amino-*β*-CD.

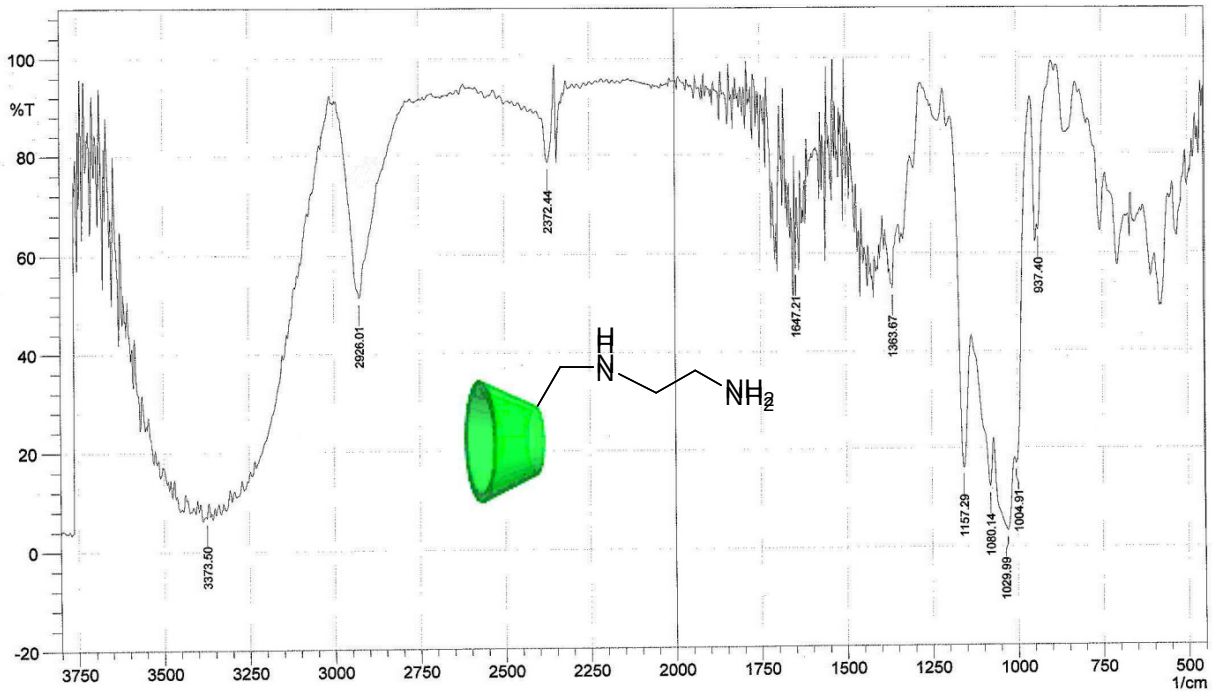

Figure S6.6. IR spectrum of 6-mono-(*N*-aminoethyl) amino-*β*-CD.

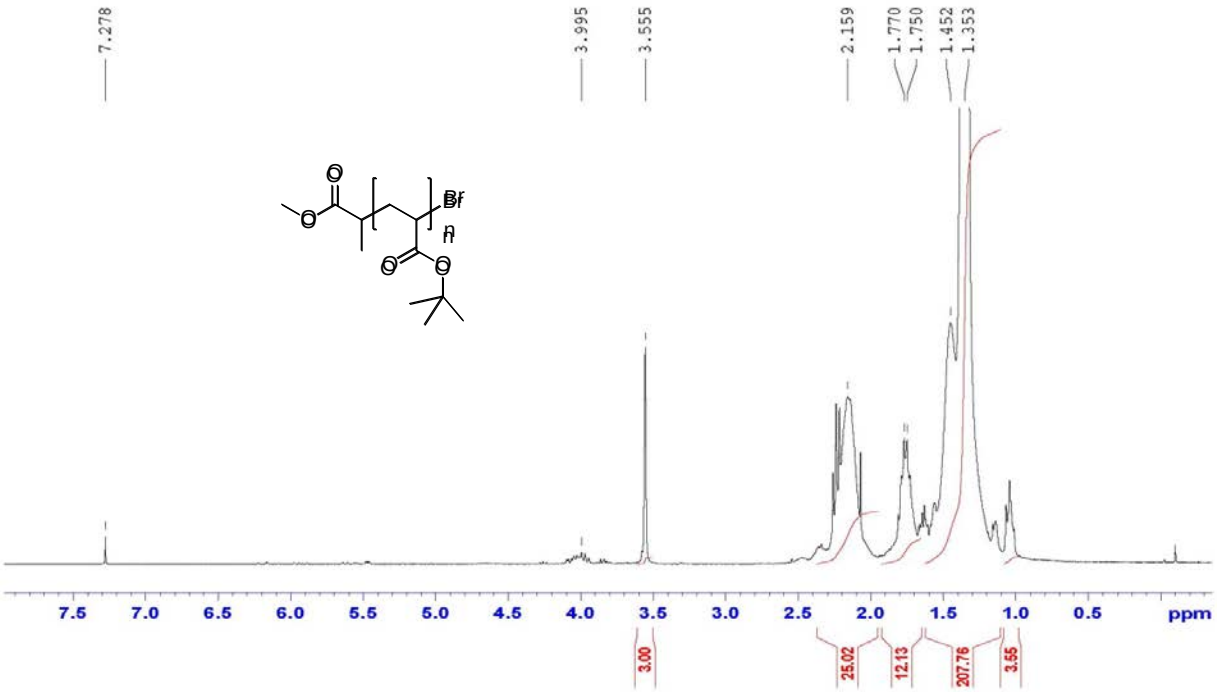

Figure S6.7. ^{1}H NMR spectrum of poly(*tert*-butyl acrylate).

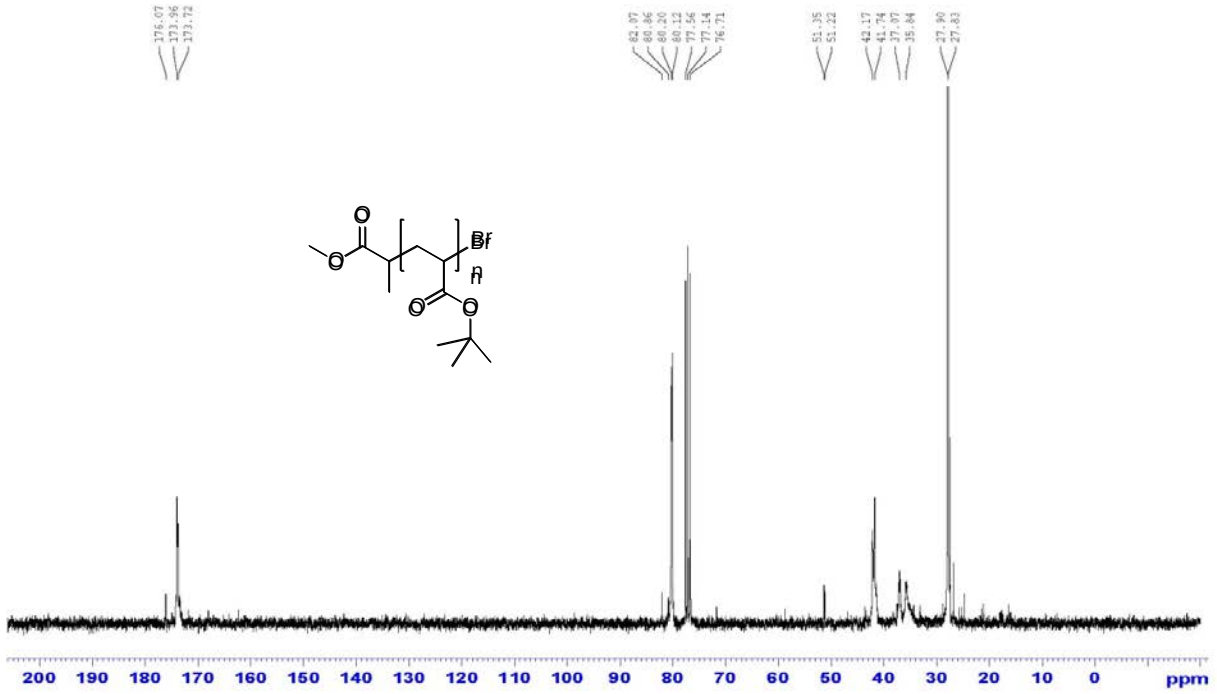

Figure S6.8. ^{13}C NMR spectrum of poly(*tert*-butyl acrylate).

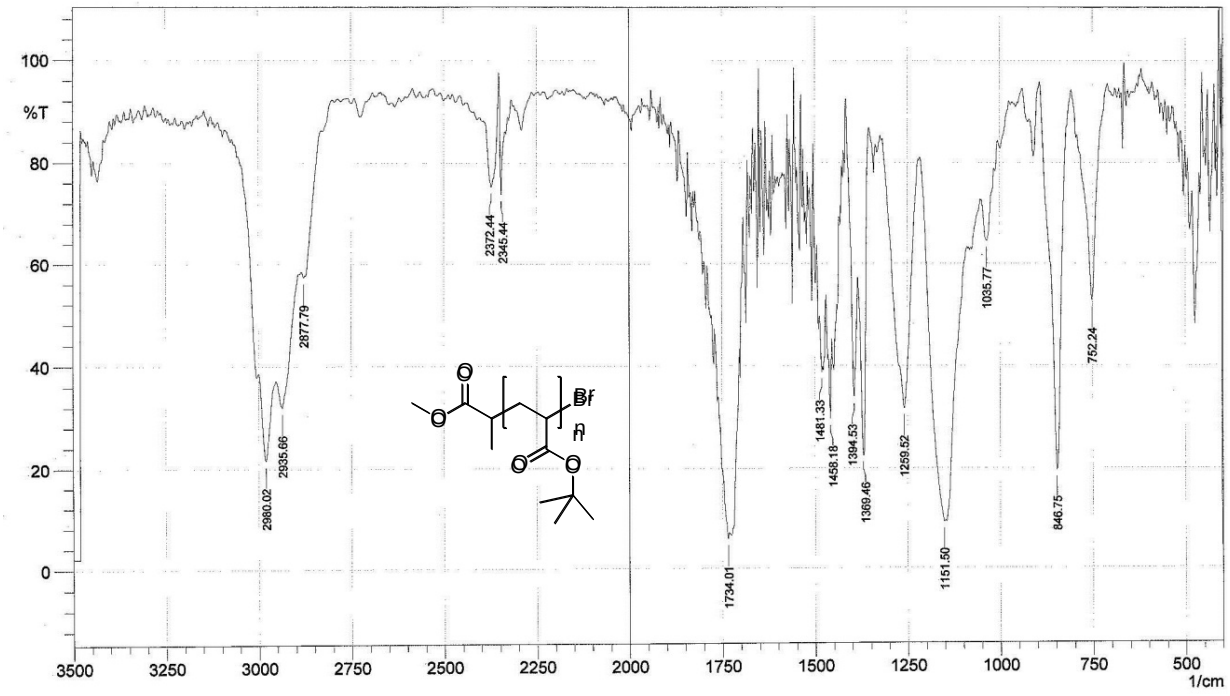

Figure S6.9. IR spectrum of poly(*tert*-butyl acrylate).

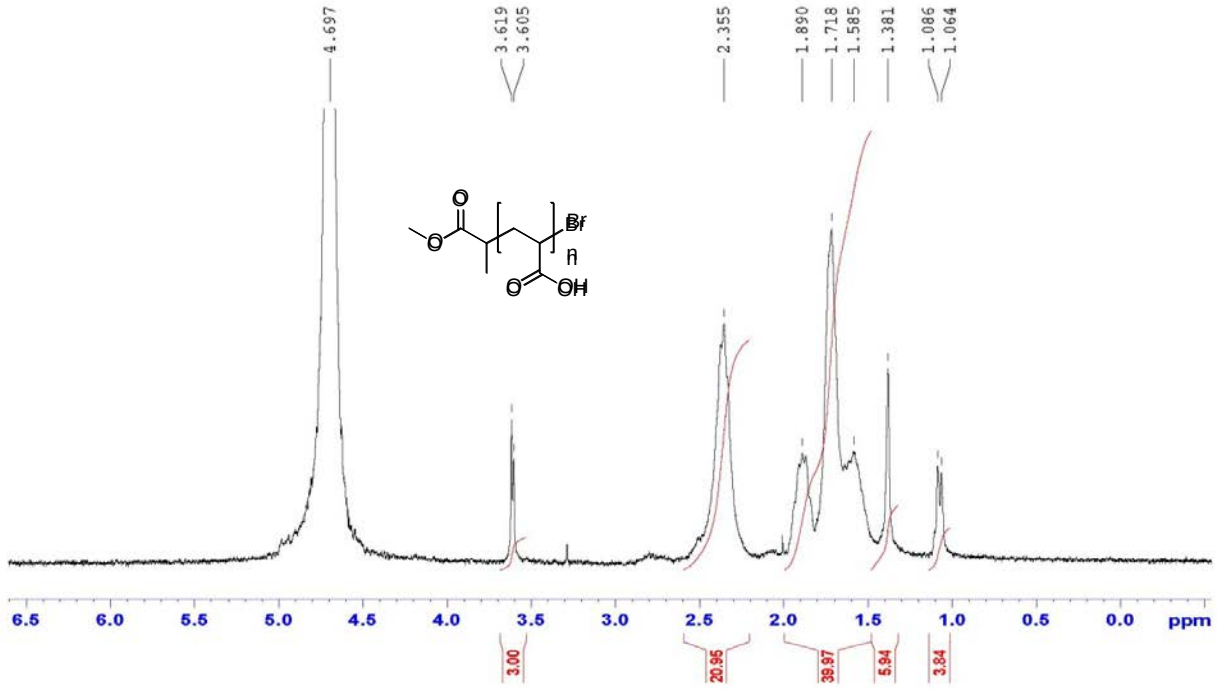

Figure S6.10. ^{1}H NMR spectrum of polyacrylic acid.

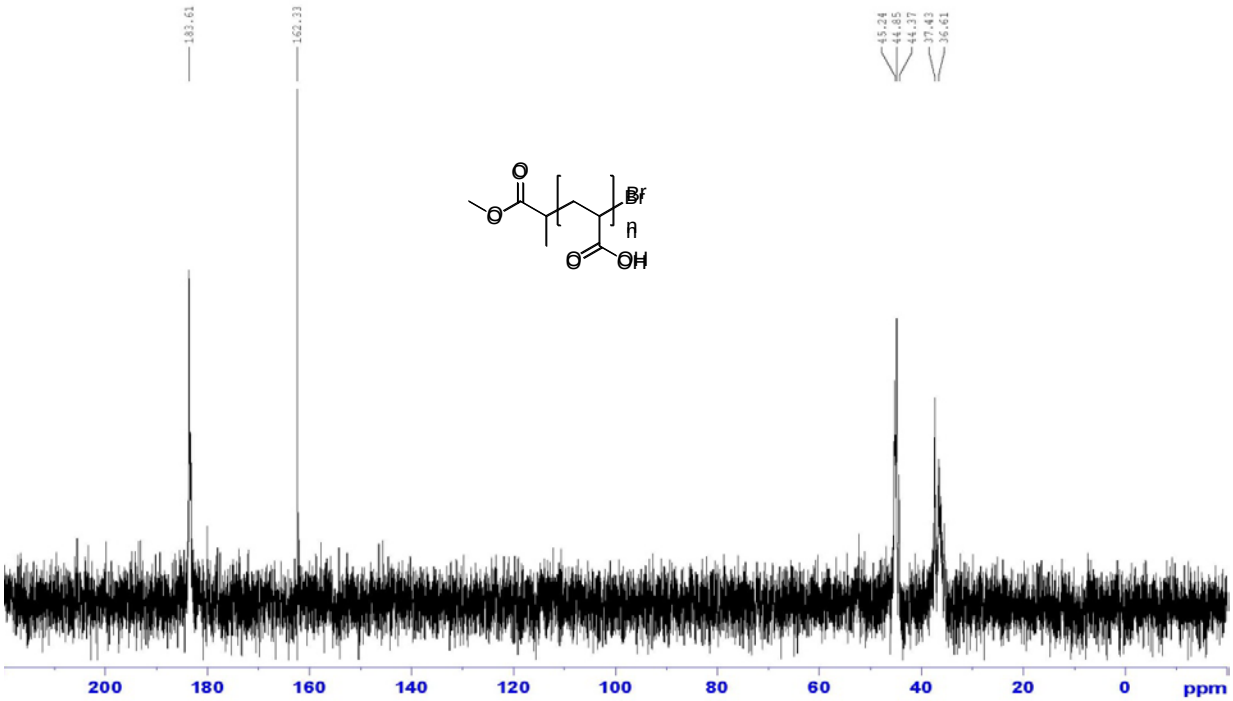

Figure S6.11. ^{13}C NMR spectrum of polyacrylic acid.

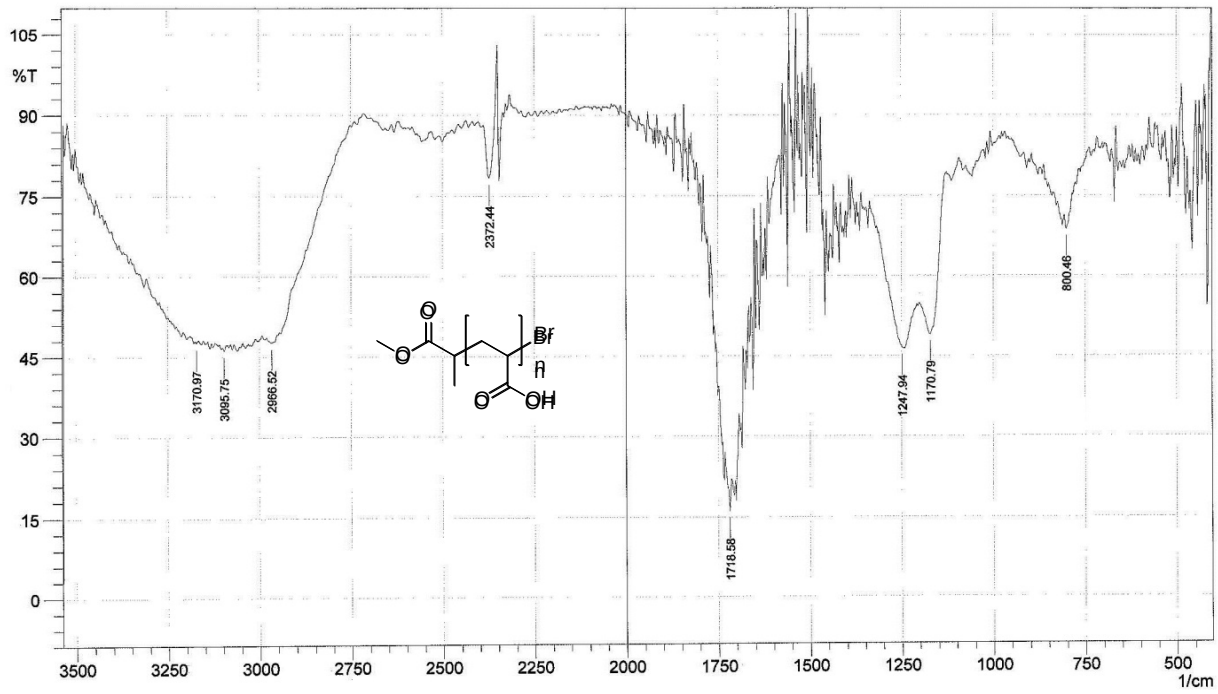

Figure S6.12. IR spectrum of polyacrylic acid.

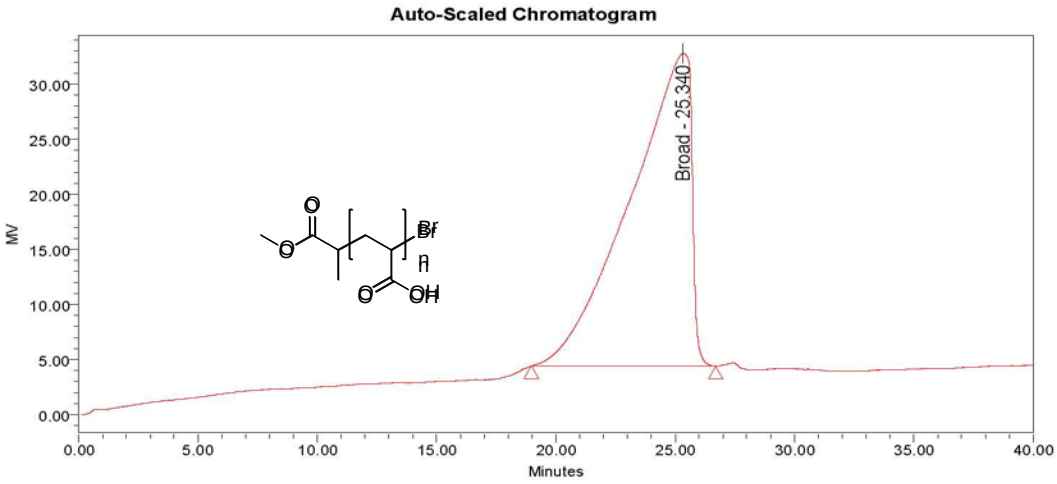

GPC Results

	Dist Name	Mn	Mw	Mv	MP	Mz	Mz+1	Polydispersity	K	alpha
1										
2		785	833			896	974	1.062216		
3										
4										

Figure S6.13. GPC chromatogram and result of polyacrylic acid.

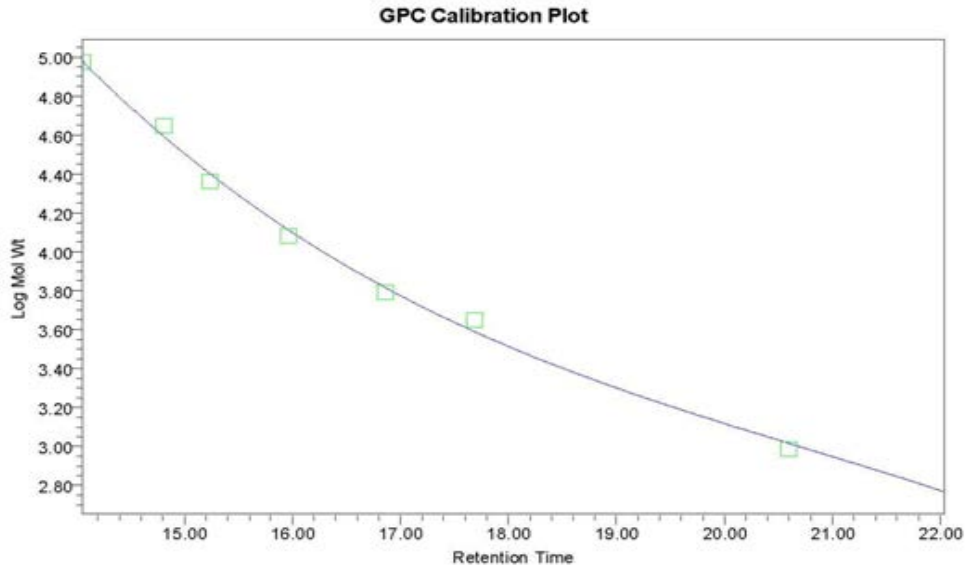

GPC Calibration Table

	Mol Wt (Daltons)	Retention Time (min)	Calculated Weight (Daltons)	% Residual
1	94000	14.053	95474	-1.543
2	44400	14.812	39069	13.644
3	23000	15.235	25185	-8.677
4	12000	15.965	12923	-7.145
5	6240	16.862	6525	-4.369
6	4450	17.687	3883	14.597
7	970	20.598	1036	-6.325
8	600	22.036	584	2.666

Figure S6.14. Calibration plot of GPC with PEG standards.

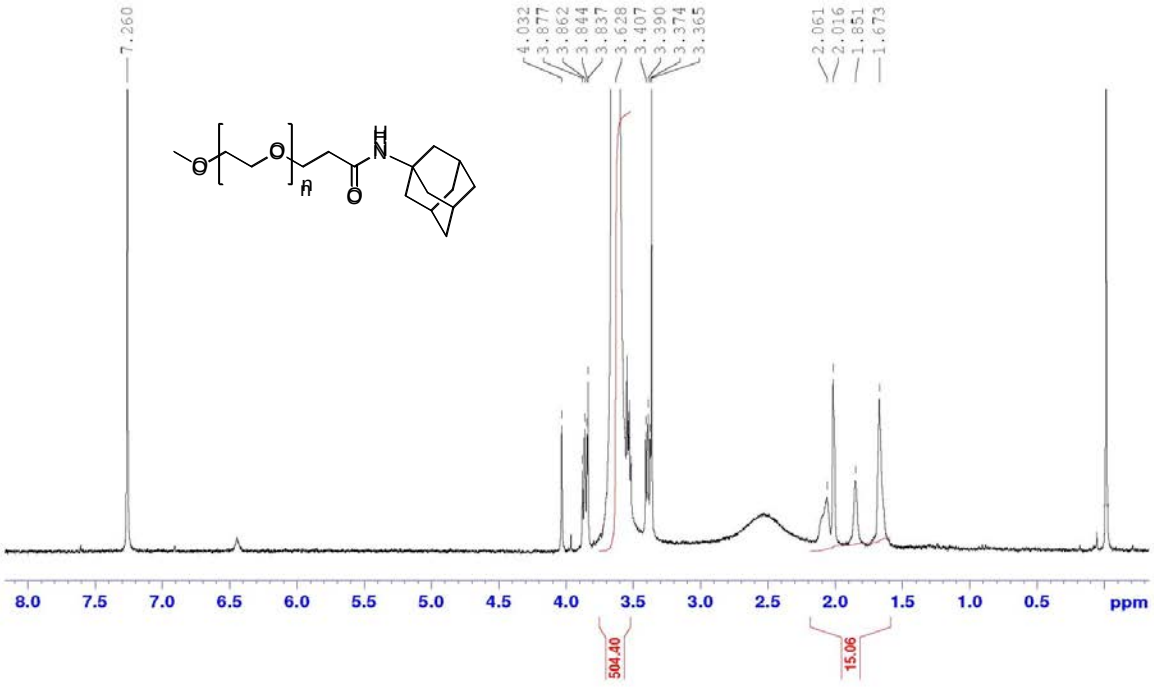

Figure S6.15. ^{1}H NMR spectrum of PEG-AD.

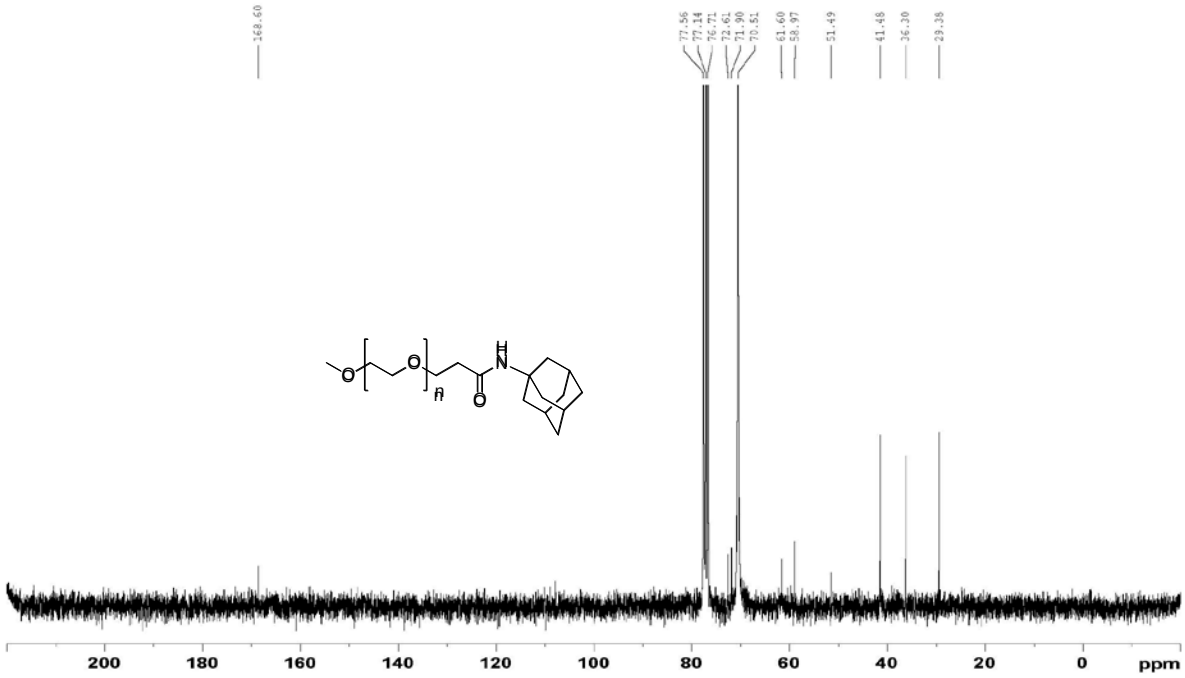

Figure S6.16. ^{13}C NMR spectrum of PEG-AD.

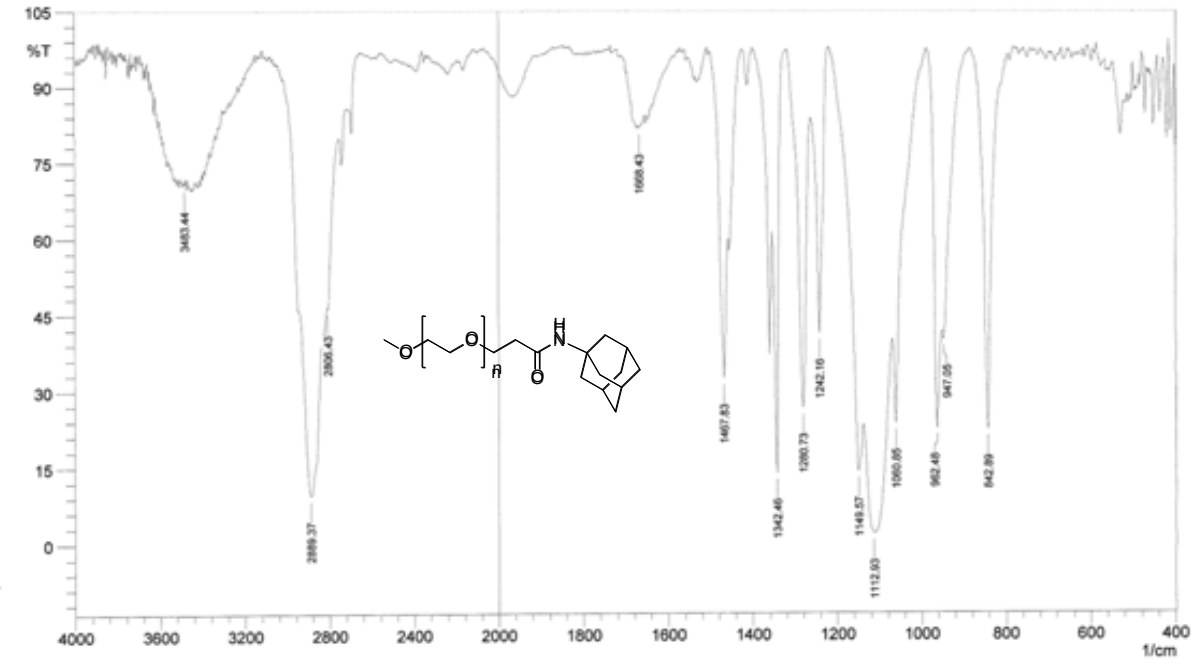

Figure S6.17. IR spectrum of PEG-AD.

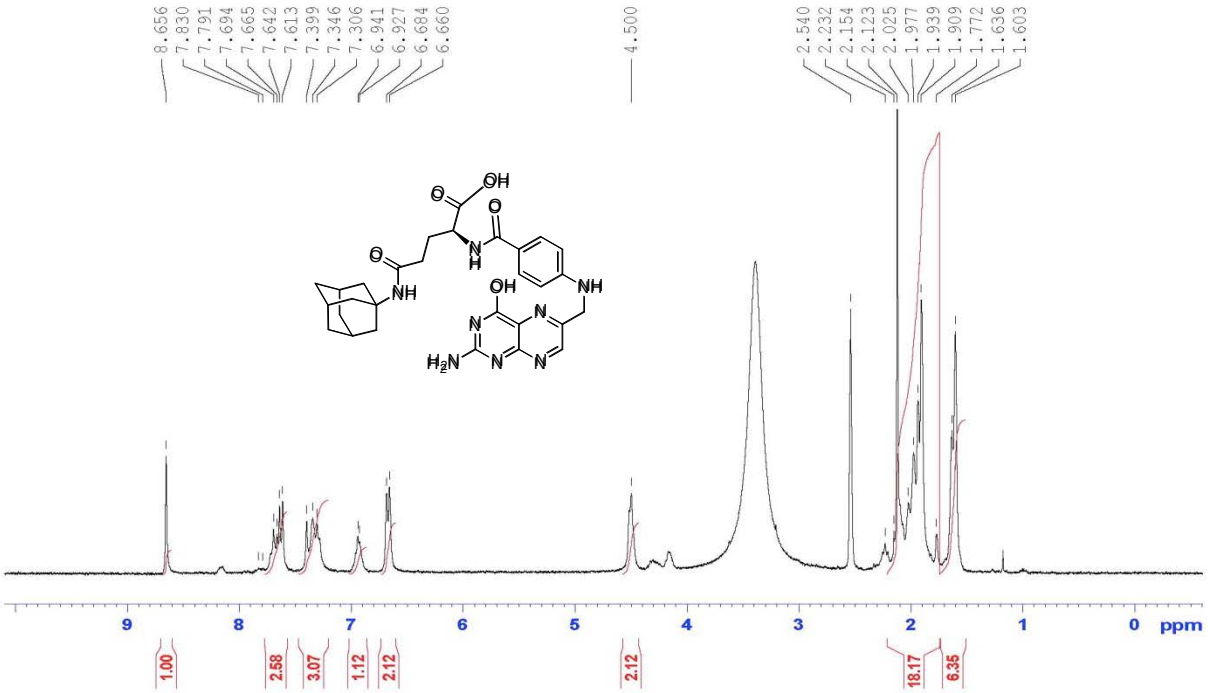

Figure S6.18. ^{1}H NMR spectrum of FA-AD.

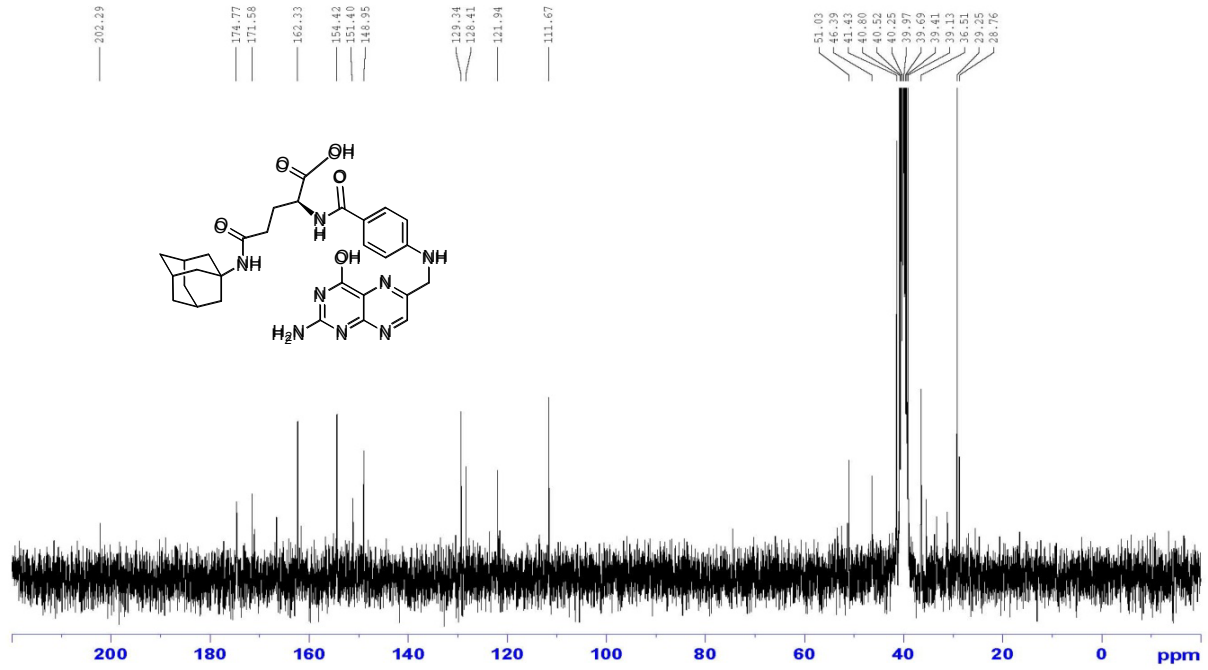

Figure S6.19. ^{13}C NMR spectrum of FA-AD.

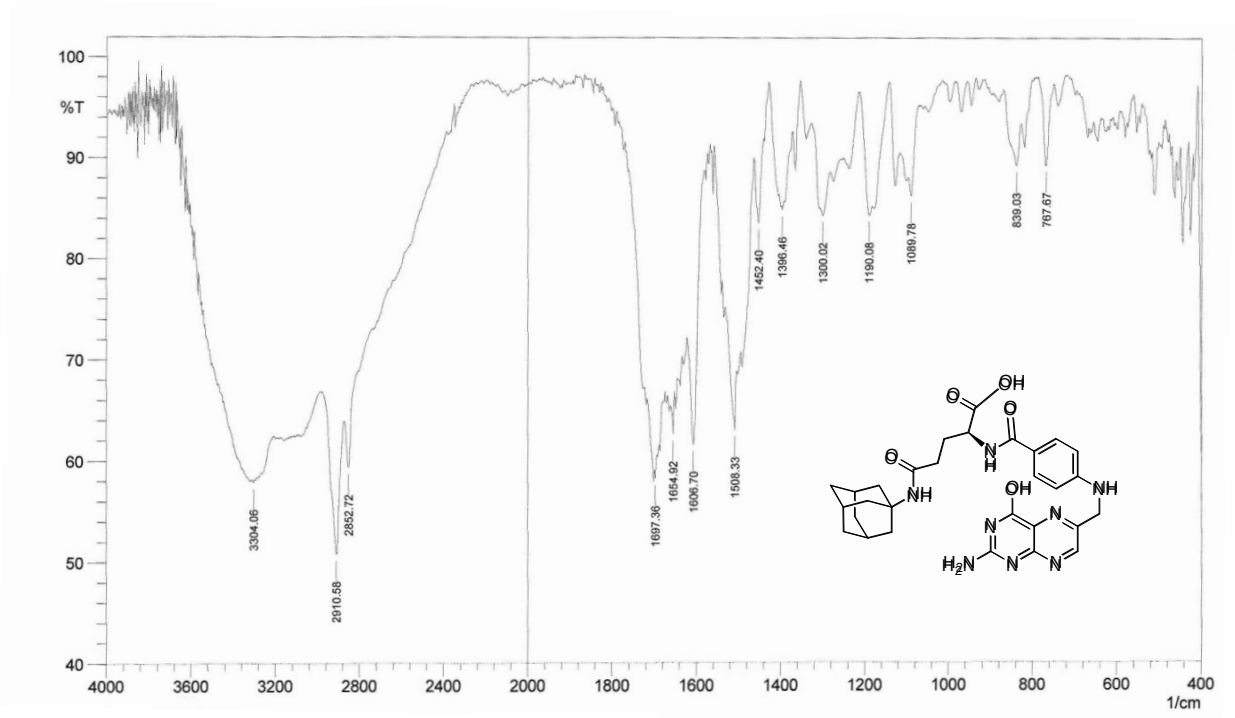

Figure S6.20. IR spectrum of FA-AD.

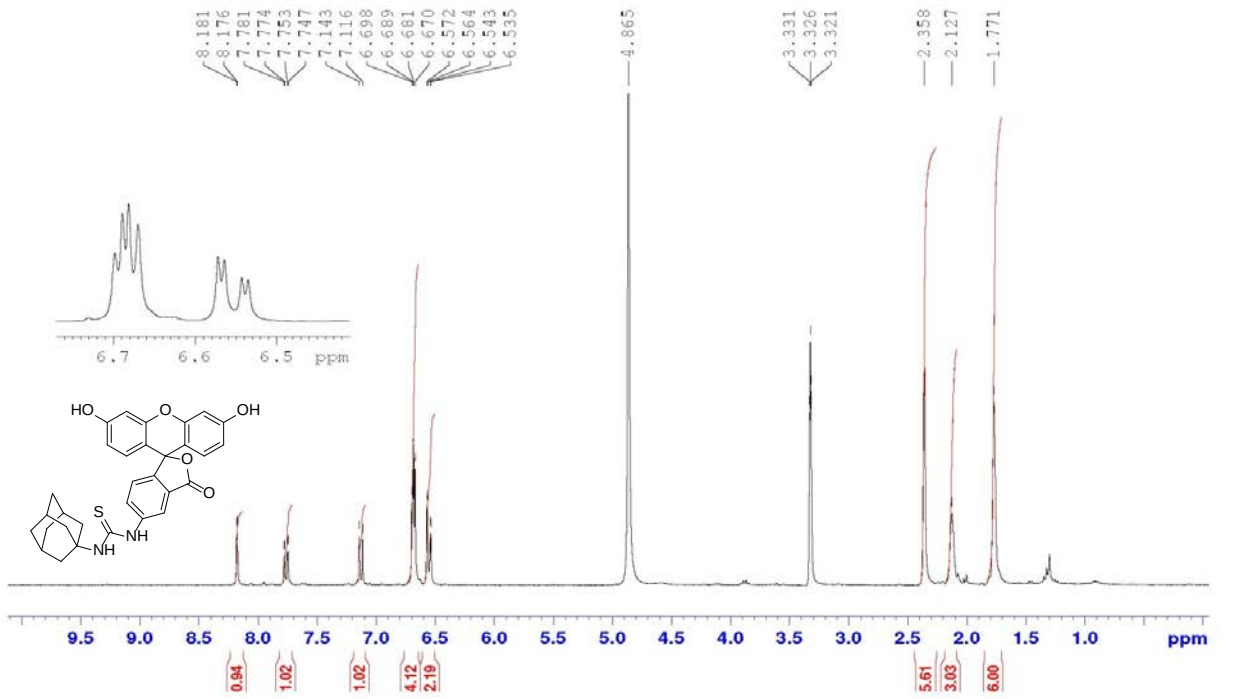

Figure S6.21. ^{1}H NMR spectrum of FITC-AD.

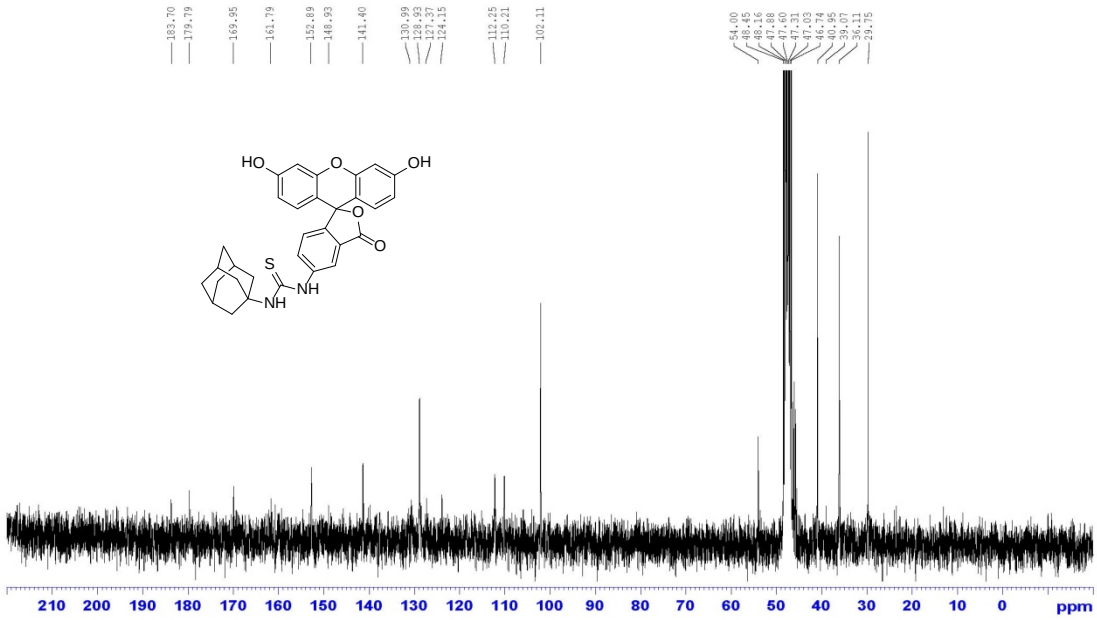

Figure S6.22. ^{13}C NMR spectrum of FITC-AD.

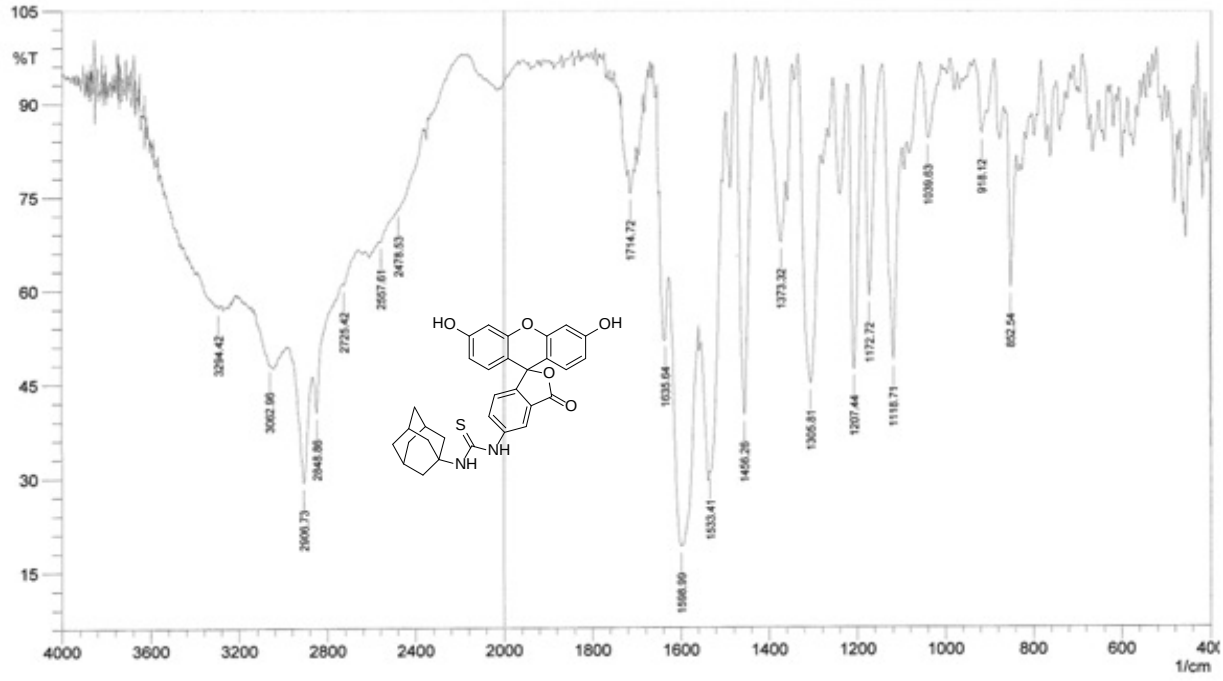

Figure S6.23. IR spectrum of FITC-AD.

7. References:

(1) R. C. Petter, J. S. Salek, C. T. Sikorski, G. Kumaravel and F. T. Lin, *J. Am. Chem. Soc.*, 1990, **112**, 3860.

(2) S.-P. Tang, P. Hu, H.-Y. Chen, S. Chen, Z.-W. Mao and L.-N. Ji, *J. Mol. Catal. A: Chem.*, 2011, **335**, 222.

(3) Y. Zhen, S. Wan, Y. Liu, H. Yan, R. Shi and C. Wang, *Macromol. Chem. Phys.*, 2005, **206**, 607.

(4) H. Wang, S. Wang, H. Su, K.-J. Chen, A. L. Armijo, W.-Y. Lin, Y. Wang, J. Sun, K.-i. Kamei, J. Czernin, C. G. Radu and H.-R. Tseng, *Angew. Chem. Int. Ed.*, 2009, **48**, 4344.

(5) S. Dhar, Z. Liu, J. Thomale, H. Dai and S. J. Lippard, *J. Am. Chem. Soc.*, 2008, **130**, 11467.

(6) L. Zhu, D. Zhang, D. Qu, Q. Wang, X. Ma and H. Tian, *Chem. Commun.*, 2010, **46**, 2587.